Review of research on Arctic sea ice physics based on the Chinese National Arctic Research Expedition

LEI Ruibo[1*], ZHANG Zhanhai[1], LI Zhijun[2], YANG Qinghua[3], LI Bingrui[1] & LI Tao[4]

[1] SOA Key Laboratory for Polar Science, Polar Research Institute of China, Shanghai 200136, China;
[2] State Key Laboratory of Coastal and Offshore Engineering, Dalian University of Technology, Dalian 116024, China;
[3] SOA Key Laboratory of Research on Marine Hazards Forecasting, National Marine Environmental Forecasting Center, Beijing 100081, China;
[4] College of Oceanic and Atmospheric Sciences, Ocean University of China, Qingdao, 266100, China

Abstract   China launched its Arctic research program and organized the first Chinese National Arctic Research Expedition (CHINARE-Arctic) in 1999. By 2016, six further expeditions had been conducted using the R/V *Xuelong*. The main region of the expeditions has focused on the Pacific sector of the Arctic Ocean for sea ice observations. The expeditions have used icebreaker, helicopter, boat, floe, and buoy platforms to perform these observations. Some new technologies have been developed, in particular, the underway auto-observing system for sea ice thickness using an electromagnetic instrument. The long-term measurement systems, e.g., the sea ice mass balance buoy, allow observations to extend from summer to winter. Some international cooperation projects have been involved in CHINARE-Arctic, especially the "Developing Arctic Modeling and Observing Capabilities for Long-Term Environmental Studies" project funded by the European Union during the International Polar Year. Arctic sea ice observations have been used to verify remote sensing products, identify changes in Arctic sea ice, optimize the parameterizations of sea ice physical processes, and assess the accessibility of ice-covered waters, especially around the Northeast Passage. Recommendations are provided as guidance to future CHINARE-Arctic projects. For example, a standardized operation system of sea ice observations should be contracted, and the observations of sea ice dynamics should be enhanced. The upcoming launch of a new Chinese icebreaker will allow increased ship time in support of future CHINARE Arctic oceanographic investigations.

Keywords   sea ice, observation, Arctic, CHINARE, climate change

1   Introduction

In recent decades, warming has been more prominent in the Arctic than in the mid-latitudes, which is a pattern known as Arctic amplification (Serreze et al., 2009; Overland et al., 2014). Consequently, the extent and volume of Arctic sea ice has declined dramatically in recent decades as the surface air temperature increased. The sea ice extent has been declining at a rate of ~3.8% per decade, whereas the perennial ice has declined at a much greater rate of ~11.5% per decade from 1979 to 2012 (Comiso and Hall, 2014). In September 2012, the Arctic sea ice extent reached a record minimum since 1979, with a reduction of 45% compared with the 1979–2010 climatology (Parkinson and Comiso, 2013). Combined analysis using submarine and ICESat data

* Corresponding author, Email: leiruibo@pric.org.cn

has revealed that the average sea ice thickness over the Arctic Basin at the end of the melt season for the years 2003–2008 has decreased by 1.6 m relative to that during 1958–1976 (Kwok and Rothrock, 2009). Between the ICESat (2003–2008) and CryoSat-2 (2010–2011) periods, the autumn volume declined by 4291 km^3 and the winter volume by 1479 km^3 (Laxon et al., 2013). Between autumn 2010 and 2012, there was a 14% reduction in the Arctic sea ice volume (Tilling et al., 2015). The Arctic-wide melt season has lengthened at a rate of 5 d·decade^{-1} from 1979 to 2013 (Stroeve et al., 2014). A continuation of these sea ice changes will increase the amount of light penetrating the Arctic Ocean, enhance sea ice melt, and affect sea ice and upper ocean ecosystems (Arrigo et al., 2012). Increased ice melt combined with surface convergence caused by wind has freshened the Beaufort Gyre (Krishfield et al., 2014). The decrease in Arctic sea ice cover is caused by many factors (Serreze et al., 2007), which include atmospheric warming (Overland et al., 2008), atmospheric circulation (Wang et al., 2009), shifts in cloud feedback (Kay et al., 2008) and albedo feedback (Perovich et al., 2011), advected ocean heat (Woodgate et al., 2010), and heat from river inflow (Nghiem et al., 2014).

It was suggested recently that both the warming and the loss of sea ice in the Arctic have had an impact on atmospheric pressure fields. As the west–east component of the wind speed weakens, the north–south meanders in the atmospheric jet stream are expected to become more prominent (Bhatt et al., 2014). Modeling studies support the association between Arctic warming and colder winters over the United States and much of Eurasia (Petoukhov and Semenov, 2010; Liu et al., 2012). Changes in the Arctic climate and the loss of Arctic sea ice have considerable influence on the climate and extreme weather in China (Wu et al., 2009). The shrinking and thinning of Arctic sea ice also allow greater accessibility for shipping. Numerical models have indicated that because of the decrease in sea ice, the probability of open-water vessel transit via the NEP in September was approximately 40% in 1979–2005, but that it had increased to 61%–71% in 2006–2015 (Smith and Stephenson, 2013).

From space, passive microwave sensors can collect sea ice measurements during the night and they are widely independent of cloud cover. The sea ice concentration data acquired from the Advanced Microwave Scanning Radiometer onboard EOS (AMSR-E; launched in 2002) and its successor, AMSR2, have a spatial resolution (6.25 km) that is a factor of four finer than the SMMR-SSMIS data. However, it is remains inadequate for the applications of navigation and climate modeling. Moreover, during the melting season, its accuracy decreases significantly because of the weakening of the contrast between open water and melt pond over the ice (Beitsch et al., 2015). Sea ice thickness can be estimated from data acquired by the spaceborne altimeters. Nevertheless, the decommissioning of ICESat in 2009, coupled with the delayed launch of

ICESat-2, suggests there will be a significant gap in ice thickness measurements. The launch of CryoSat-2 in April 2010 might provide altimetry data to fill this gap. However, because of sea ice surface melt, spaceborne altimeters cannot measure the ice freeboard accurately, and ice thickness data are not available during summer.

The Coupled Model Intercomparison Project (e.g., CMIP3 and CMIP5) studies have provided projections of sea ice loss. The sea ice extent derived from CMIP5 matches the observations more closely than that from the CMIP3 models (Stroeve et al., 2012). Based on the CMIP5 models, Liu et al. (2013) predicted that, between 2054 and 2058, the summer Arctic will reach an ice-free state, defined as an ice area of less than one million km^2. However, the trends of sea ice loss in most CMIP5 models are still slower than the observed decline. This might be because most of the data informing predictive models have been derived for thick and old ice (Eicken, 2013). We know little about the physical processes that govern the current mix of young and old ice.

China launched its Arctic research program and organized the first Chinese National Arctic Research Expedition (CHINARE-Arctic) in 1999. Another six expeditions were conducted using the R/V *Xuelong* in 2003, 2008, 2010, 2012, 2014, and 2016. A quasi-operational stage has been reached since the International Polar Year in 2007–2008 as the CHINARE-Arctic was implemented every second year afterwards. A series of field experiments was undertaken during the expeditions to identify changes in Arctic sea ice and to characterize interactions among the atmosphere, sea ice, and the upper ocean from floe to basin scale. For sea ice observations, the main study regions of the CHINARE-Arctic, except for the 5th CHINARE-Arctic, focused on the Pacific sector of the Arctic Ocean (PSA), including the Chukchi Sea, Chukchi Cap, Canadian Basin, and Alpha Ridge. The Northeast Passage (NEP) regions were also involved in the 5th CHINARE-Arctic. The data collected by ship-, helicopter-, camp-, and buoy-based sea ice measurements during the expeditions have been used to verify remote sensing products, optimize the parameterizations of sea ice physics, which are applied to sea ice numerical models, and assess the accessibility of the Arctic ice-covered waters, especially the regions around the NEP. Some international cooperation projects have also been involved in CHINARE-Arctic, notably the project "Developing Arctic Modeling and Observing Capabilities for Long-Term Environmental Studies" funded by the European Union during the International Polar Year. Scientists from the United States, Finland, Estonia, Japan, and Iceland have joined the sea ice team at times during the CHINARE-Arctic program.

Here, we review the research of Arctic sea ice physics based on CHINARE-Arctic from 1999 to 2016. This includes the development of both technologies for sea ice observation applied during the cruise and procedures for research on the changes in Arctic sea ice, interactions
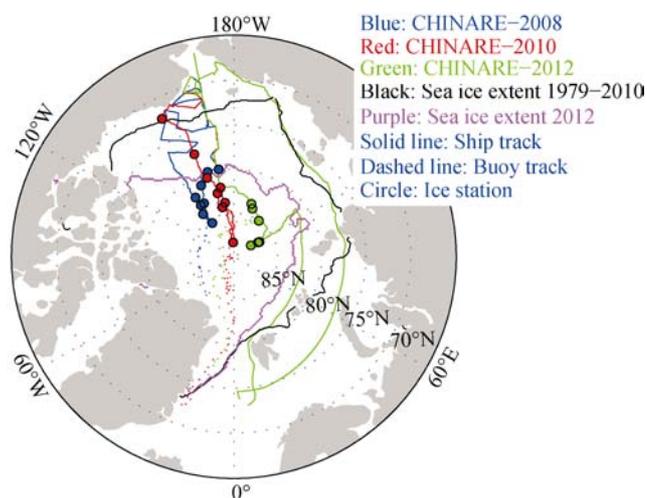
Figure 1 Tracks of the R/V *Xuelong* and the buoys, and the locations of the ice stations, in the 3rd, 4th, and 5th CHINARE-Arctic programs. The Arctic sea ice extent in September 2012 and its climatology during 1981–2010 are also shown.

among the atmosphere, sea ice, and the ocean, parameterizations of Arctic sea ice physical processes and their applications in numerical modeling, and ground verification of satellite remote sensing.

2   Processes in research on Arctic sea ice physics

2.1   Technologies for sea ice observation

Icebreaker, helicopter, boat, floe, and buoy platforms have been used for Arctic sea ice observations during the CHINARE-Arctic. Shipborne observations provide a snapshot of the spatial distribution of sea ice morphological parameters, including its concentration, thickness, and surface features at local to regional scales. These observations can provide a wider perspective than *in situ* observations and permit detection of small-scale features not resolved by satellite measurements. Therefore, they represent a bridge between satellite and *in situ* observations. The greatest advance for ship-based sea ice measurement was the underway auto-observing system for sea ice thickness using an electromagnetic instrument (Xie et al., 2013; Lei et al., 2017). This instrument (EM31-ICE), together with a GPS receiver, sonic ranging sensor, and laser altimeter, is fixed in a fiberglass-reinforced frame that enables stable deployment to a height of 4.0 m above the waterline beyond the ship's hull. The sonic ranger and laser altimeter are used to measure the distance between the instrument and the snow/water surface. The EM31 measures the apparent conductivity to obtain the distance between the sensor and the ice–water interface. Combining the measurements, the total thicknesses of snow and sea ice can then be obtained. This system has been used to measure sea ice thickness since the 2nd CHINARE-Arctic in 2003.

As a supplement for the EM31 measurement, a downward-looking video is mounted on the port size of the icebreaker to determine the scale of the stratigraphic cross section of the ice block and thus, the thickness of level ice. In addition to the instrument used to measure sea ice thickness, other apparatus are used to observe other physical parameters of sea ice. For example, the surface temperatures of water or sea ice can be measured by a downward-looking infrared thermometer (Lei et al., 2017). The measurement of surface temperature is used to identify the melt stage of the ice surface.

An aerial survey is an effective addition to shipborne observations because it can avoid the track taken by an icebreaker, which generally is the path of least resistance and fewest pressure ridges. To conduct aerial surveys, an equipment package containing a digital camera, portable GPS, and an altimeter is mounted outside the helicopter in a downward-facing orientation. Based on the brightness and color of the aerial image, the surface characteristics are partitioned into three components: snow-covered ice, melt ponds, and open water. This system has been used in every CHINARE-Arctic since 2003. In particular, eight helicopter flights were undertaken and more than 9000 aerial images were obtained during the 3rd CHINARE-Arctic in 2008. The areal fractions of open water, melt ponds, and ice cover were then obtained along the cruise tracks between 77°N and 86°N (Lu et al., 2010). An object-based classification algorithm was developed to automatically extract sea ice and melt ponds from aerial photographs, which effectively resolves the time-consuming and labor-intensive problems of the manual delineation process (Miao et al., 2015).

During each CHINARE-Arctic, several short-term ice stations and one ice camp were set up. The major work at the short-term ice stations (lasting approximately 4 h) was the collection of samples used to determine the texture and physical structure of the snow and ice (Lei et al., 2012a; Huang et al., 2013; Huang et al., 2016a). The major work at the ice camp (lasting approximately 10 d) was the measurement of the synoptic processes of the interactions among the atmospheric boundary layer, snow, ice, and upper ocean, and the deployment of long-term measurement systems, e.g., the ice-tethered buoy and the automatic weather station. The synoptic measurements included radiation and turbulent fluxes between air and ice (Bian et al., 2003; Cheng et al., 2008), the snow and ice mass balance (Xie et al., 2013; Lei et al., 2017), transmission of irradiance by snow and sea ice (Zhao et al., 2009; Lei et al., 2012a), and the physical structure of the upper ocean (Lei et al., 2011; Guo et al., 2015). Some new platforms were designed to support the observations of the radiation transmission by sea ice or melt ponds, and of their mass balance (Zhao et al., 2009; Huang et al., 2011; Lei et al., 2012a). Dynamic interactions between sea ice and the ocean are strongly dependent on sea ice bottom morphology. A ground-based EM31 can measure sea ice thickness with

higher spatial resolution than a shipborne EM31 (Xie et al., 2013). However, it cannot provide data on the ice surface and bottom morphology separately. Upward-looking sonar (ULS) onboard an underwater vehicle can map ice bottom morphology with high spatial resolution. Therefore, the combined use of an EM31 and a ULS is an optimal method with which to characterize the sea ice morphology fully. This method was adopted using an Autonomous and Remotely operated underwater Vehicle (ARV) during the 6th CHINARE-Arctic (Lei et al., 2017). A floe-referenced navigation method for the ARV operation under the ice was developed using an inertial navigation system.
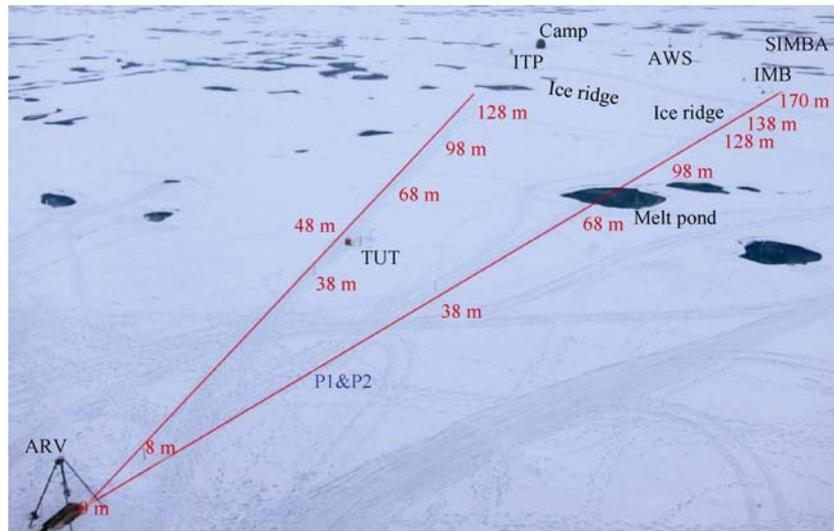
Figure 2 The ice camp established during the 6th CHINARE-Arctic. The deployed instruments included the ARV, Ice-Tethered Profile (ITP), Automatic Weather Station (AWS), snow buoy of the Taiyuan University of Technology (TUT), sea Ice Mass balance Buoy (IMB), and Snow and Ice Mass Balance Array (SIMBA). Also shown are the measurement profiles of ice thickness by the ARV, EM31, and boreholes (P1 & P2) (repainted from the Figure 2 in Lei et al., 2017).

Because the CHINARE-Arctic was implemented in summer, when the sea ice was in the melting phase, some of the auxiliary technologies for the refreezing of boreholes used for the equipment deployment were applied to the measurement of sea ice mass balance during the ice camp (Li et al., 2004). Moreover, the long-term measurement system extended the observations of CHINARE-Arctic from summer to winter. For example, the conductive and oceanic heat fluxes and the mass balance of sea ice from late summer to the following early summer were investigated using an IMB deployed in the Arctic Ocean during the 3rd CHINARE-Arctic (Lei et al., 2014). Four ice-tethered buoys deployed in the region near the North Pole in the 4th CHINARE-Arctic were used to investigate sea ice motion and deformation from the central Arctic to Fram Strait (Lei et al., 2016a).

The presence of sea ice is clearly the main factor influencing shipping safety in the Arctic Ocean. The engineering properties of sea ice are therefore important for the design of ships. Conducting mechanical strength tests of sea ice onboard the ship, rather than transporting the ice sample ashore, can preserve the sea ice samples in their original condition. For research ships not equipped with a cold laboratory, such as the R/V *Xuelong*, a mobile cold laboratory could be installed onboard. Thus, a mobile cold laboratory has been designed with a lowest refrigeration temperature of −30°C. This cold laboratory also includes a thermotank to preserve ice samples at below the required temperature. Some uniaxial compression tests of ice samples have been performed within this laboratory during the most recent CHINARE-Arctic programs (Han et al., 2015).

2.2 Changes in Arctic sea ice status

Combining historical data collected from the same region using consistent observation methods helps identify long-term change of the Arctic sea ice condition. For example, many marine science voyages have covered the PSA since 1994 (Tucker et al., 1999; Li et al., 2005; Perovich et al., 2009; Lei et al., 2012a; 2017; Xie et al., 2013). Ship-based observations of sea ice in this region show that sea ice loss in summer has clearly occurred since 2007, evidenced by the northward retreat of the marginal ice zone (MIZ) and the significantly low sea ice concentration observed in the central Arctic Ocean (Figure 3). However, there have also been large interannual variations due to the forcing of the atmospheric circulation. For example, larger inflow of multiyear ice during winter, less sea ice melt in the subsequent summer, and earlier sea ice refreezing in the autumn likely initiated a feedback loop for the ice season of 2013–2014. This was because the Arctic Oscillation had strong negative polarity during September 2013–August 2014, which resulted in the heavy sea ice condition observed during the 6th CHINARE-Arctic in the summer of 2014 (Lei et al., 2017).
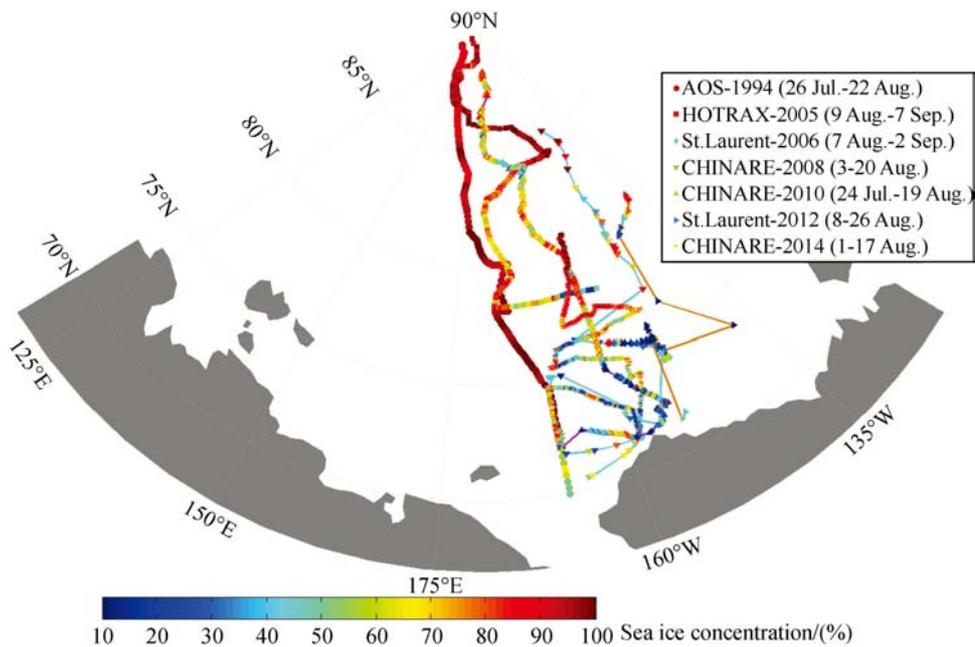
Figure 3   Sea ice concentration measured by marine science voyages operated in the PSA since 1994.

Aerial surveys revealed that a significantly higher coverage of melt ponds were observed in the PSA in the summer of 2008 compared with that observed in 2003 (Lu et al., 2010). The albedo in this region was markedly smaller than reported in earlier studies because of an overall decrease in ice concentration and an increase in melt ponds. In particular, anomalously low ice concentration (~75%) was observed in the high Arctic (above 88°N) in late summer 2010, which characterized the unusual transpolar reduction of sea ice (Huang et al., 2016b). The SSM/I sea ice concentration and the CLARA black-sky albedo were used to estimate sea ice albedo in the PSA. In July–August 1982–2009, the linear trend of the ice albedo was –0.046 units per decade (Lei et al., 2016b). During 1 June to 19 August, the melting of sea ice resulted in an increase of solar heat input to the ice-ocean system of 282 MJ·m^{-2} from 1982 to 2009. The physical characterization of the ice-albedo feedback can be obtained not only by aerial or remote sensing observations at basin scale but also by *in situ* measurements at floe scale. Sea ice thickness measurements at the ice camp during the 4th CHINARE-Arctic showed the ice surrounding melt ponds melted more rapidly than snow-covered ice. This was because more solar radiation was transmitted into the upper ocean in areas including melt ponds than in areas of snow-covered ice (Xie et al., 2013).

The shrinking and the thinning of Arctic sea ice allow greater accessibility for shipping. Combined data of remote sensing measurements and ship-based observations during the 5th CHINRARE-Arctic cruise showed that sea ice conditions in the Arctic NEP have changed dramatically over the past four decades. Data for October–November showed that spatially averaged ice thickness in the NEP decreased from 1.2–1.3 m in

2003–2006 to 0.2–0.6 m in 2011–2012. As the result of decreasing multiyear ice, thinning ice, and delayed freeze-up, the spatially averaged length of the open period (ice concentration <50%) increased from 84 d in the 1980s to 114 d in the 2000s and it reached 146 d in 2012 (Lei et al., 2015). The summer sea ice along the high-latitude sea route to the north of the eastern Arctic islands also decreased during the past decade; the ice-free period reached 42 d in 2012. This sea route avoids shallow waters along the coast, and it improves access to the Arctic sea route for deep-draft vessels.

Most of the evidence of Arctic sea ice loss has been observed at the surface, e.g., the retreat of sea ice extent, increase in melt pond coverage, and darkening of the Arctic Ocean surface resulting from the decrease of albedo. Physical measurements of sea ice cores from 2008 to 2012 have revealed that the Arctic sea ice inclusion (brine/gas matrix) volume has increased in the ice interior because of the strengthened ice-albedo feedback and lengthened ice melt season (Huang et al., 2016a). Consequently, the total Arctic sea ice mass is reduced at the end of the summer melt. Therefore, the volumetric fraction of sea ice inclusions can be considered as an alternative indicator of Arctic sea ice reduction.

2.3   Interactions among the atmosphere, sea ice, and ocean

Atmospheric boundary layer data (wind, air temperature, relative humidity, and the upward and downward components of the shortwave and longwave radiation) measured at the ice camp during the 2nd CHINARE-Arctic were used to force a 1D thermodynamic model (Cheng et al., 2008). Snow and sea ice mass balance data were used to

validate the model results. The model indicated that good simulation of snow thickness evolution depends strongly on the accuracy of the modeled snowmelt. A time-dependent surface albedo parameterization was critical for the seasonal evolution of snow and ice thickness. The application of 15–20 model levels of snow and ice was recommended for the following reasons. (1) It ensured good reproduction of the vertical snow/ice temperature profile even when solar radiation was large. (2) It decreased the sensitivity of the snow and ice mass balance to changes in surface albedo. (3) It enabled the calculation of subsurface melting of snow and ice. (4) It reasonably reproduced the superimposed ice formation and onset of ice melt. This study highlighted that accuracy of atmospheric forcing was more important than model resolution, which suggested the importance of *in situ* observations because they could support the optimization of atmospheric reanalysis products.

The data collected by an IMB deployed during the 3rd CHINARE-Arctic in summer 2008 (Figure 4) was used to study seasonal changes in the sea ice mass balance and to estimate the oceanic heat flux based on the residual energy method (Lei et al., 2014). The results showed that the competition between oceanic and conductive heat fluxes dominated the low-frequency variations of ice growth. However, the high-frequency variation in ice growth was controlled largely by the oceanic heat flux. From mid-November 2008 to mid-June 2009, the average oceanic heat flux along a track from 86.2°N, 115.2°W to 84.6°N, 33.9°W was 7.1 W·m^{-2}. The relatively high oceanic heat flux (10–15 W·m^{-2}) observed during the autumn and early winter can be attributed to the summer warming of the surface ocean. Upward mixing of warm deep water, observed when the IMB drifted over the shallow region of the Lomonosov Ridge (85.4°–85.9°N, 52.2°–66.4°W), demonstrated the impact of bathymetry on the oceanic heat flux under ice cover, and consequently, on the basal ice mass balance.
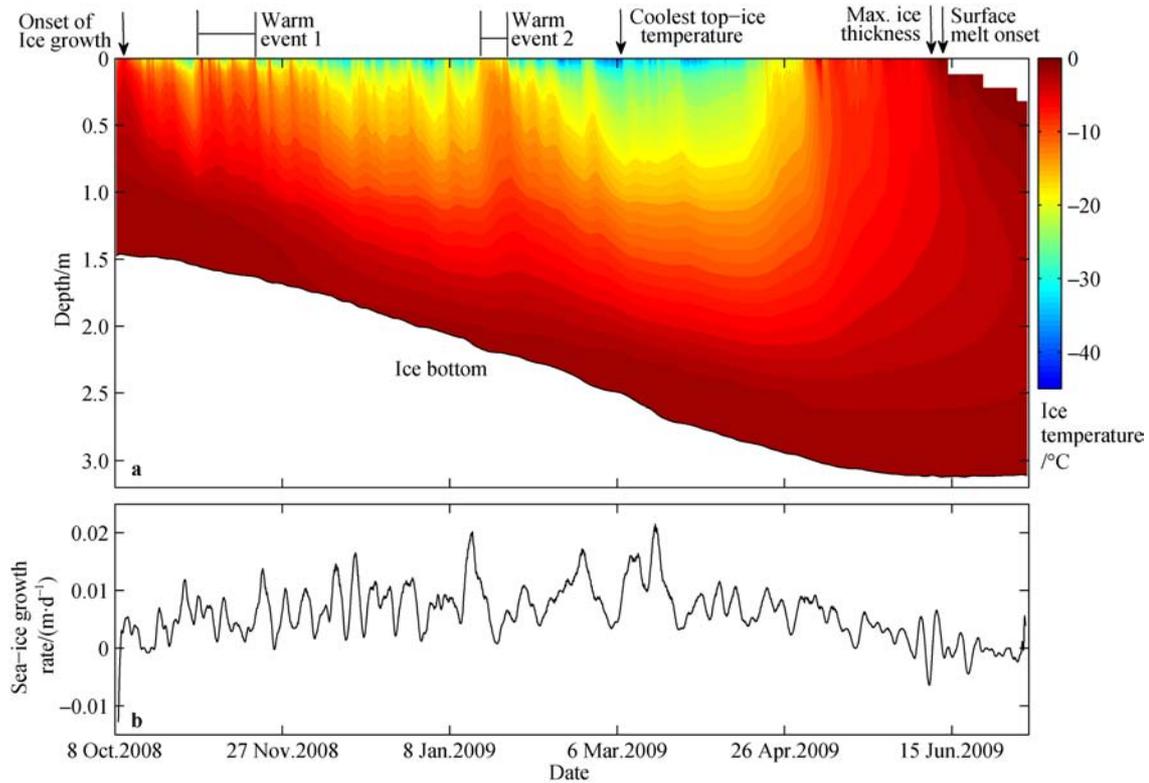
Figure 4 Evolution of sea ice internal temperature (**a**), and growth rate (**b**) measured by the IMB deployed during the 3rd CHINARE-Arctic in summer 2008 (repainted from the Figure 3 in Lei et al., 2014).

The loss of Arctic sea ice area, increase of open water, and fragmentation of ice floes during summer introduces greater lateral ice melt and enhances the thermodynamic interactions between floes and leads. The thermodynamic processes of a system involving a floe and a small lead in the central Arctic were investigated during the ice camp of the 3rd CHINARE-Arctic in late August 2008 (Lei et al., 2011). The measurements included surface air temperatures above the floe, spectral albedo of the lead, seawater temperatures in the lead and under the ice cover, and lateral and bottom mass balance of the floe. By the end of the measurements, the thickness of the investigated floe had reached its annual minimum, while the lateral edge of the floe was still in the melt stage, with a mean melting rate of 0.01 m·d^{-1} during the measurement. This implied that lateral melting of the floe made a more significant contribution to the ice mass balance than surface and bottom melting by the end of August.

To understand the role of solar radiation quantitatively, considerable efforts have been devoted to understand the temporal development of the albedo of sea ice with various surface types (Perovich et al., 2002). Compared with surface albedo measurements, there are relatively few measurements of the transmission and absorption of solar irradiance by Arctic sea ice, because of the difficulty of deploying optical sensors within/under sea ice. Field measurements of the reflection and transmission of irradiance by the combined snow and sea ice layers were performed at an ice camp and several short-term stations established in the PSA above 80°N during the 4th CHINARE-Arctic in summer 2010 (Lei et al., 2012b). The integrated 350–920 nm albedo ranged from 0.54 to 0.88, and it was found dependent primarily on the geophysical properties of snow but not on those of sea ice. This implied that all snow cover remained optically thick, even though snow melting had commenced at all measurement sites. For sea ice about 1.66-m thick and covered by 2.5–8.5 cm of snow at the ice camp, the integrated 350–920 nm transmittance ranged from 0.017 to 0.065, and 29.2% of the incident solar irradiance was absorbed and used to melt the snow and sea ice. Rapid snow melting resulted from a light drizzle that doubled the available solar irradiance under the ice, which further accelerated ice bottom decay. This highlights the importance of the form of precipitation on Arctic ice-albedo feedback. An increase in the moisture content of Arctic snowfall due to climate warming and increase in open water during summer will enhance the ice-albedo feedback, contributing to the loss of Arctic sea ice.

2.4 Parameterizations of Arctic sea ice physical processes

Surface albedo was observed at the ice camp during the 3rd CHINARE-Arctic. Based on the *in situ* data, several albedo parameterizations were incorporated into a 1D high resolution thermodynamic snow–sea ice model to simulate local surface albedo (Yang et al., 2011). The observed albedo varied between 0.75 and 0.85 during the observation period. Using the observed wind, air temperature, relative humidity, longwave radiation, and incident shortwave radiation to force the model, the trend of the observed albedo was captured by an albedo parameterization that took snow and ice thickness into account. However, it still could not reconstruct the short-term variability because of the precipitation or changes in sky conditions.

To characterize the heat budget of the melt pond surface, observations of the depth, shape, and surface condition of melt ponds, radiation properties, air temperature, wind speed, and relative humidity were undertaken at the ice camp during 4th CHINARE-Arctic in summer 2010. These data were used to calculate downward and upward shortwave/longwave radiation, and to parameterize the sensible and latent heat fluxes (Zhang et al., 2014). The results show that the turbulent heat flux was more than twice the net longwave radiation when the air temperature was <0°C. More than 50% of the radiation energy entering the pond surface was absorbed by the pond water. A thin ice layer formed on the pond surface when the air temperature was <0°C. Only a small percentage (5.5%) of solar radiation was absorbed by such a thin ice layer.

Based on an investigation of the uniaxial compressive properties of samples of Arctic summer sea ice collected during the 5th CHINARE-Arctic, the dependence of the uniaxial compressive strength on a number of parameters, including physical indices (porosity and density) of the ice, the loading (stress) rate, and the experimental temperature were discussed (Han et al., 2015). The total porosity of the sea ice ranged from 150×10^{-3} to 330×10^{-3}. The uniaxial compressive strength decreased linearly with an increase in the total porosity. Ice porosity can be used as a physical index to estimate the uniaxial compressive strength. The density of the ice has an inverse relationship with the total porosity; therefore, density can be used to parameterize the uniaxial compressive strength.

2.5 Ground verification of satellite remote sensing

Remote sensing product of sea ice thickness is not available in summer. Ground verification of satellite remote sensing has been performed only for sea ice concentration using the CHINARE-Arctic data collected by ship-based measurements (Xie et al., 2013) and by aerial surveys (Lu et al., 2010; Huang et al., 2016b; Li et al., 2017). According to ship-based visually observed ice concentrations and AMSR-E ice concentrations, there was a reasonable match of the overall pattern of lower concentration in the MIZ and higher concentration in the pack ice zone (PIZ) between the two datasets. However, the AMSR-E ice concentrations were generally greater than those observed visually in the PIZ, and less than those observed in the MIZ, resulting in an R^2 of 0.53 for the entire cruise during the 4th CHINARE-Arctic (Xie et al., 2013). The deviation can be attributed to the fact that most small floes in the MIZ and small leads in the PIZ cannot be identified by microwave remote sensing with relatively low resolution.

The ice concentrations derived from aerial images collected from the 3rd CHINARE-Arctic in summer 2008 and the AMSR-E products were comparable with each other, especially in the range of 50%–90%. However, the satellite-derived data overestimated the aerial observations by 14% ± 9% in areas with large ice concentrations (>90%), and almost missed those with very low ice concentrations (<20%) (Lu et al., 2010). The ice concentrations detected from the aerial images and AMSR-E data at 87.0°–87.5°N in summer 2010 also exhibited similar spatial patterns, although the AMSR-E concentration was approximately 18% higher than that of the aerial images (Li et al., 2017). This can be attributed to the 6.25-km resolution of AMSR-E, which cannot separate melt ponds/submerged ice from open

water and cannot detect small leads between floes. Thus, aerial observations play an important role in providing high-resolution independent estimates of ice concentration and area fraction of melt ponds to validate and/or supplement spaceborne remote sensing products, especially in the region near the North Pole.

3　Scientific highlights

Based on the research on Arctic sea ice physics using the CHINARE-Arctic platform, the Chinese sea ice community acquired the following new scientific knowledge, which has contributed to the research of rapid changes of Arctic climate and sea ice:

(1) The most significant decline of summer Arctic sea ice extent has occurred in the PSA from the Beaufort Sea to the East Siberian Sea. In July–August 1982–2009, the linear trend of the composite albedo and sea ice albedo was –0.069 and –0.046 units·decade^{-1}, which was about twice as large in magnitude relative to the entire Arctic Ocean. The decrease in sea ice albedo can be attributed to earlier onset of surface melt, delayed onset of surface freezing, and increased melt pond coverage in summer.

(2) Multiyear ice concentration in the PSA prior to the melt season can be significantly related to the Arctic Oscillation index. A negative winter Arctic Oscillation can be associated with higher inflow of multiyear ice advected from north of the Canadian Arctic Archipelago, which might act against the retreat of sea ice in the PSA. Conversely, under positive polarity of the summer Arctic Dipole Anomaly, enhanced southerly winds can bring more warm air from the south and advect northward greater amounts of sea ice from the PSA. Therefore, high positive polarity of the summer Arctic Dipole Anomaly is related to a reduction in area of summer sea ice in the PSA, consequently, favors the opening of the NEP.

(3) The loss of summer Arctic sea ice might increase the heat storage of the upper ocean during summer and early autumn, which might consequently increase the oceanic heat flux under the ice and delay the growth of winter sea ice.

(4) The Arctic amplification of climate warming might increase precipitation in the form of rainfall in summer for Arctic regions, which could enhance the surface melt of snow and sea ice, and further enhance the sea ice-albedo feedback.

4　Prospects

The PSA is the main research region for the CHINARE-Arctic programs. In this region, if observations could be extended to the region north of 88°N, as achieved during the 4th CHINARE-Arctic, the scientific value of the observations would be of greater significance because remote sensing products are not available there. Such data

could be used to adjust and validate numerical simulations.

Standardized operations of ship- and helicopter-based sea ice observations using the same protocol are conducive to the incorporation of the CHINARE-Arctic fieldwork within the international network. For example, the protocol of the Arctic Shipborne Sea Ice Standardization Tool was established by the Climate–Cryosphere Arctic Sea Ice Working Group. This protocol has been used in the CHINARE-Arctic program since 2010. Thus, Chinese ship-based sea ice observations have been incorporated within the international project "Ice Watch", coordinated by the University of Alaska Fairbanks, USA.

For the application of *in situ* data to numerical simulations, most studies focus on the parameterizations of sea ice thermodynamic modeling. This is because observations of sea ice dynamic processes, e.g., sea ice deformation, floe fragmentation, interactions between waves and the ice, and between cyclones and the ice, are relatively difficult to achieve and thus, such data are scarce. Recent decades have seen pronounced reduction in sea ice volume and a dramatic increase in summer open-water area. The combination of increased ice-free area and more mobile ice cover has led to dramatic dynamic processes. It is therefore necessary to increase investigation of ice–ocean–atmosphere dynamics. Since the 6th CHINARE-Arctic, arrays of ice-tethered buoys have been deployed in the Beaufort Gyre region, which can be used to monitor the processes of sea ice deformation and floe fragmentation under the forces of cyclones that had been identified to increase in strength (Simmonds et al., 2009). The next step is to launch a novel mixture of autonomous technologies (ice-tethered instruments, floats, drifters, and gliders) in the MIZ to resolve changes in the physics associated with the increasing expanse of open water, and to focus on the interactions between sea ice and waves. These data could be used further used to optimize the parameterization schemes in dynamic numerical models.

For the application of *in situ* data to the ground verification of satellite remote sensing, only data of sea ice concentration have been used. However, the next stage will be to apply other parameterizations. For example, the melt pond coverage obtained by ship- and helicopter-based observations could be used to validate the melt pond products retrieved by the optical instruments of the Moderate Resolution Imaging Spectroradiometer (Rösel et al., 2012). Data of sea ice motion, collected by ice-tethered buoys, can be used to validate the related products derived from microwave measurements (Spreen et al., 2011). The snow and sea ice mass balance data measured by IMBs can be used to validate the snow depth products derived by passive microwave remote sensing (Markus et al., 2006) and the ice thickness product derived by spaceborne altimeters (Laxon et al., 2013). When ground verification of satellite remote sensing products is performed using *in situ* data, differences in the spatial and temporal resolutions should be taken into consideration.

The sea ice forecasting service is important for the operation of both scientific cruises and commercial shipping in the Arctic Ocean. Ensemble based data assimilation techniques for sea ice physical parameters have been developed and applied in forecasting (Yang et al., 2014a; 2015; 2016). A short-term forecast system of Arctic sea ice has been established (Yang et al., 2014b), which has provided forecasting services to the field operations of CHINARE-Arctic and Chinese commercial vessels, e.g., the M/V *Yongsheng*, during the use of the NEP. The commercial use of the Arctic NEP by Chinese stakeholders has entered a practical stage. From 2013 to 2016, there were nine voyages using this sea route by Chinese commercial ships. To improve the quality of the sea ice forecasting service, interactive information exchange between online users, i.e., the ships in the Arctic Ocean, and the forecasting system is necessary. The most valuable information obtained from online users is real-time *in situ* data of sea ice, e.g., sea ice concentrations and thicknesses obtained by ship-based observations. If these real-time data could be transferred swiftly and incorporated in the initialization of the numerical model, the forecasting service could be improved further.

The CHINARE-Arctic programs are multidisciplinary cruises. Thus, the study of the interactions of various earth system processes and interdisciplinary research should be strengthened. In particular, the influence of the changes in Arctic sea ice and other physical environmental parameters on the marine ecosystem has been receiving increased attention from the international scientific community. Interdisciplinary research could promote greater understanding of such changes in the Arctic Ocean.

Currently, only one icebreaker, the R/V *Xuelong*, is available for the oceanographic investigations by CHINARE-Arctic in regions covered by sea ice. The ice breaking level of the R/V *Xuelong* is Polar Class 6. Thus, it can perform summer/autumn operations in medium first-year ice that might include some old ice inclusions, and it can continuously break level ice of 1.2-m thick, including a 0.2-m-thick snow cover. This restricts the study region of the CHINARE-Arctic program to central Arctic Ocean when sea ice is heavy. In addition, the complex logistics associated with the supply of personnel and materials to Antarctic stations also limits the ship time invested for Arctic oceanographic investigation. Fortunately, a new icebreaker is under construction, which will be launched and available for CHINARE-Arctic program in 2019/2020. The ice breaking level of this new icebreaker is Polar Class 3, which means it will be able to perform fieldwork in regions with heavy sea ice. Consequently, the icebreaker group, comprising the R/V *Xuelong* and the new icebreaker, will effectively increase the available ship time in support of Arctic oceanographic investigations by CHINARE-Arctic.

References

Arrigo K R, Perovich D K, Pickart R S, et al. 2012. Massive phytoplankton blooms under Arctic sea ice. Science, 336(6087): 1408–1408

Beitsch A, Kern S, Kaleschke L. 2015. Comparison of SSM/I and AMSR-E sea ice concentrations with ASPeCt ship observations around Antarctica. IEEE Trans Geosci Remote Sens, 53(4): 1985–1996

Bhatt U S, Walker D A, Walsh J E, et al. 2014. Implications of Arctic sea ice decline for the Earth system. Annu Rev Environ Resour, 39(1): 57–89

Bian L G, Gao Z Q, Lu L H, et al. 2003. Observational estimation of heat budgets on drifting ice and open water over the Arctic Ocean. Sci China Ser D Earth Sci, 46(6): 580–591

Cheng B, Zhang Z H, Vihma T, et al. 2008. Model experiments on snow and ice thermodynamics in the Arctic Ocean with CHINARE 2003 data. J Geophys Res, 113(C9): C09020, doi: 10.1029/2007JC004654

Comiso J C, Hall D K. 2014. Climate trends in the Arctic as observed from space. Wiley Interdiscip Rev Climate Change, 5(3): 389–409

Eicken H. 2013. Ocean science: Arctic sea ice needs better forecasts. Nature, 497(7450): 431–433

Guo G J, Shi J X, Jiao Y T. 2015. Temporal variability of vertical heat flux in the Makarov Basin during the ice camp observation in summer 2010. Acta Oceanol Sin, 34(11): 118–125

Han H W, Li Z J, Huang W F, et al. 2015. The uniaxial compressive strength of the Arctic summer sea ice. Acta Oceanol Sin, 34(1): 129–136

Huang W F, Li Z J, Wang Y X, et al. 2011. A concept for autonomous and continuous observation of melt pond morphology: Instrument design and test trail during the 4th CHINARE-Arctic in 2010. Adv Polar Sci, 22(4): 273–280

Huang W F, Lei R B, Ilkka M, et al. 2013. The physical structures of snow and sea ice in the arctic section of 150°–180°W during the summer of 2010. Acta Oceanol Sin, 32(5): 57–67

Huang W F, Lei R B, Han H W, et al. 2016a. Physical structures and interior melt of the central Arctic sea ice/snow in summer 2012. Cold Reg Sci Technol, 124: 127–137

Huang W, Lu P, Lei R, et al. 2016b. Melt pond distribution and geometry in high Arctic sea ice derived from aerial investigations. Ann Glaciol, 57(73): 105–118

Kay J E, L'Ecuyer T, Gettelman A, et al. 2008. The contribution of cloud and radiation anomalies to the 2007 Arctic sea ice extent minimum. Geophys Res Lett, 35(8): L08503, doi: 10.1029/2008GL033451

Krishfield R A, Proshutinsky A, Tateyama K, et al. 2014. Deterioration of perennial sea ice in the Beaufort Gyre from 2003 to 2012 and its impact on the oceanic freshwater cycle. J Geophys Res, 119(2): 1271–1305

Kwok R, Rothrock D A. 2009. Decline in Arctic sea ice thickness from submarine and ICESat records: 1958–2008. Geophys Res Lett, 36(15): L15501, doi: 10.1029/2009GL039035

Laxon S W, Giles K A, Ridout A L, et al. 2013. CryoSat-2 estimates of Arctic sea ice thickness and volume. Geophys Res Lett, 40(4): 732–737

Lei R B, Li Z J, Cheng B, et al. 2011. Investigation of the thermodynamic processes of a floe-lead system in the central Arctic during later summer. Adv Polar Sci, 22(1): 10–16

Lei R B, Zhang Z H, Ilkka M, et al. 2012a. Reflection and transmission of irradiance by snow and sea ice in the central Arctic Ocean in summer 2010. Polar Res, 31(1): 17325, doi: 10.3402/polar.v31i0.17325

Lei R B, Li Z J, Li N, et al. 2012b. Crucial physical characteristics of sea ice in the Arctic section of 143°–180°W during August and early September 2008. Acta Oceanol Sin, 31(4): 65–75

Lei R B, Li N, Heil P, et al. 2014. Multiyear sea ice thermal regimes and oceanic heat flux derived from an ice mass balance buoy in the Arctic Ocean. J Geophys Res, 119(9): 537–547, doi: 10.1002/2012JC008731

Lei R B, Xie H J, Wang J, et al. 2015. Changes in sea ice conditions along the Arctic Northeast Passage from 1979 to 2012. Cold Reg Sci Technol, 119: 132-144

Lei R B, Heil P, Wang J, et al. 2016a. Characterization of sea-ice kinematic in the Arctic outflow region using buoy data. Polar Res, 35(1): 22658, doi: 10.3402/polar.v35.22658

Lei R B, Tian-Kunze X, Leppäranta M, et al. 2016b. Changes in summer sea ice, albedo, and portioning of surface solar radiation in the Pacific sector of Arctic Ocean during 1982–2009. J Geophys Res, 121(8): 5470–5486, doi: 10.1002/2016JC011831

Lei R B, Tian-Kunze X S, Li B R, et al. 2017. Characterization of summer Arctic sea ice morphology in the 135°-175°W sector using multi-scale methods. Cold Reg Sci Technol, 133: 108–120Li L Y, Ke C Q, Xie H J, et al. 2017. Aerial observations of sea ice and melt ponds near the North Pole during CHINARE2010. Acta Oceanol Sin, 36(1): 64–72

Li Z J, Zhang Z H, Dong X L, et al. 2004. A new technique for observing the crucial parameters of sea ice mass balance in Arctic Ocean. Prog Natl Sci, 14(9): 1077–1080 (in Chinese)

Li Z J, Zhang Z H, Lu P, et al. 2005. Some parameters in Arctic sea ice dynamics from an expedition in the summer of 2003. Acta Oceanol Sin, 24(6):54–61

Liu J P, Curry J A, Wang H J, et al. 2012. Impact of declining Arctic sea ice on winter snowfall. Proc Natl Acad Sci USA, 109(11): 4074–4079.

Liu J P, Song M R, Horton R M, et al. 2013. Reducing spread in climate model projections of a September ice-free Arctic. Proc Natl Acad Sci USA, 110(31): 12571–12576

Lu P, Li Z J, Cheng B, et al. 2010. Sea ice surface features in Arctic summer 2008: Aerial observations. Remote Sens Environ, 114(4): 693–699, doi: 10.1016/j.rse.2009.11.009

Markus T, Powell D C, Wang J R. 2006. Sensitivity of passive microwave snow depth retrievals to weather effects and snow evolution. IEEE Trans Geosci Remote Sens, 44(1): 68–77

Miao X, Xie H J, Ackley S F, et al. 2015. Object-based detection of Arctic sea ice and melt ponds using high spatial resolution aerial photographs. Cold Reg Sci Technol, 119: 211–222

Nghiem S V, Hall D K, Rigor I G, et al. 2014. Effects of Mackenzie River discharge and bathymetry on sea ice in the Beaufort Sea. Geophys Res Lett, 41(3): 873–879

Overland J E, Wang M, Salo S. 2008. The recent Arctic warm period. Tellus A, 60(4): 589–597

Overland J E, Wang M Y, Walsh J E, et al. 2014. Future Arctic climate changes: Adaptation and mitigation time scales. Earth's Fut, 2(2): 68–74.

Parkinson C L, Comiso J C. 2013. On the 2012 record low Arctic sea ice cover: Combined impact of preconditioning and an August storm. Geophys Res Lett, 40(7): 1356–1361

Perovich D K, Grenfell T C, Light B, et al. 2002. Seasonal evolution of the albedo of multiyear Arctic sea ice. J Geophys Res, 107(C10): SHE 20–1–SHE 20–13, doi: 10.1029/2000JC000438

Perovich D K, Grenfell T C, Light B, et al. 2009. Transpolar observations of the morphological properties of Arctic sea ice. J Geophys Res, 114(C1): C00A04, doi: 10.1029/2008JC004892

Perovich D K, Jones K F, Light B, et al. 2011. Solar partitioning in a changing Arctic sea-ice cover. Ann Glaciol, 52(57): 192–196

Petoukhov V, Semenov V A. 2010. A link between reduced Barents-Kara sea ice and cold winter extremes over northern continents. J Geophys Res, 115(D21): D21111, doi: 10.1029/2009JD013568

Rösel A, Kaleschke L. 2012. Exceptional melt pond occurrence in the years 2007 and 2011 on the Arctic sea ice revealed from MODIS satellite data. J Geophys Res, 117(C5): C05018, doi: 10.1029/2011JC007869

Serreze M C, Holland M M, Stroeve J. 2007. Perspectives on the Arctic's shrinking sea-ice cover. Science, 315(5818): 1533–1536

Serreze M C, Barrett A P, Stroeve J C, et al. 2009. The emergence of surface-based Arctic amplification. Cryosphere, 3(1): 11–19

Simmonds I, Keay K. 2009. Extraordinary September Arctic sea ice reductions and their relationships with storm behavior over 1979–2008. Geophys Res Lett, 36(19): L19715, doi: 10.1029/2009GL039810

Smith L C, Stephenson S R. 2013. New Trans-Arctic shipping routes navigable by midcentury. Proc Natl Acad Sci USA, 110(13): E1191–E1195

Spreen G, Kwok R, Menemenlis D. 2011. Trends in Arctic sea ice drift and role of wind forcing: 1992–2009. Geophys Res Lett, 38(19): L19501, doi: 10.1029/2011GL048970

Stroeve J C, Kattsov V, Barrett A, et al. 2012. Trends in Arctic sea ice extent from CMIP5, CMIP3 and observations. Geophys Res Lett, 39(36): L16502, doi: 10.1029/2012GL052676

Stroeve J C, Markus T, Boisvert L, et al. 2014. Changes in Arctic melt season and implications for sea ice loss. Geophys Res Lett, 41(4): 1216–1225

Tilling R L, Ridout A, Shepherd A, et al. 2015. Increased Arctic sea ice volume after anomalously low melting in 2013. Nat Geosci, 8(8): 643–646

Tucker III W B, Gow A J, Meese D A, et al. 1999. Physical characteristics of summer sea ice across the Arctic Ocean. J Geophys Res, 104(C1): 1489–1504, doi: 10.1029/98JC02607

Wang J, Zhang J L, Watanabe E, et al. 2009. Is the dipole anomaly a major driver to record lows in Arctic summer sea ice extent? Geophys Res Lett, 36(5): L05706, doi: 10.1029/2008GL036706

Woodgate R A, Weingartner T, Lindsay R. 2010. The 2007 Bering Strait oceanic heat flux and anomalous Arctic sea-ice retreat. Geophys Res Lett, 37(1): L01602, doi: 10.1029/2009GL041621

Wu B Y, Zhang R H, Wang B, et al, 2009. On the association between spring Arctic sea ice concentration and Chinese summer rainfallGeophys Res Lett, 36(9): L09501, doi: 10.1029/2009GL037299

Xie H J, Lei R B, Ke C Q, et al. 2013. Summer sea ice characteristics and morphology in the Pacific Arctic sector as observed during the CHINARE 2010 cruise. Cryosphere, 7(4): 1057–1072

Yang Q H, Cheng B, Lei R B, et al. 2011. Arctic sea ice albedo in summer: observation and modelling experiments. Acta Oceanol Sin, 33(2): 42–47 (in Chinese)

Yang Q H, Losa S N, Losch M, et al. 2014a. Assimilating SMOS sea ice thickness into a coupled ice-ocean model using a local SEIK filter. J Geophys Res, 119(10): 6680–6692

Yang Q H, Liu J P, Zhang Z H, et al. 2014b. Sensitivity of the Arctic sea ice concentration forecasts to different atmospheric forcing: a case study. Acta Oceanol Sin, 33(12): 15–23, doi: 10.1007/s13131-014-0566-7

Yang Q H, Losa S N, Losch M, et al. 2015. The role of atmospheric uncertainty in Arctic summer sea ice data assimilation and prediction. Quart J Roy Meteor Soc, 141(691): 2314–2323, doi: 10.1002/qj.2523

Yang Q H, Losch M, Losa S N, et al. 2016. Brief communication: The challenge and benefit of using sea ice concentration satellite data products with uncertainty estimates in summer sea ice data assimilation. Cryosphere, 10(2): 761–774

Zhang S G, Zhao J P, Shi J X, et al. 2014. Surface heat budget and solar radiation allocation at a melt pond during summer in the central Arctic Ocean. J Ocean Univ China, 13(1): 45–50

Zhao J P, Li T, Zhang S G, et al. 2009. The shortwave solar radiation energy absorbed by packed sea ice in the central Arctic. Adv Earth Sci, 24(1): 33–41 (in Chinese)